

# Quasi-one- and quasi-two-dimensional symbiotic solitons bound by dipolar interaction

S. K. Adhikari\*

*Instituto de Física Teórica, Universidade Estadual Paulista - UNESP, 01.140-070 São Paulo, São Paulo, Brazil*

(Dated: May 14, 2024)

We study the formation of quasi-one- (quasi-1D) and quasi-two-dimensional (quasi-2D) symbiotic solitons bound by an interspecies dipolar interaction in a binary dipolar Bose-Einstein condensate. These binary solitons have a repulsive intraspecies contact interaction stronger than the intraspecies dipolar interaction, so that they can not be bound in isolation in the absence of an interspecies dipolar interaction. These symbiotic solitons are bound in the presence of an interspecies dipolar interaction and zero interspecies contact interaction. The quasi-1D solitons are free to move along the polarization  $z$  direction of the dipolar atoms, whereas the quasi-2D solitons move in the  $x$ - $z$  plane. To illustrate these, we consider a  $^{164}\text{Er}$ - $^{166}\text{Er}$  mixture with scattering lengths  $a(^{164}\text{Er})=81a_0$  and  $a(^{166}\text{Er})=68a_0$  and with dipolar lengths  $a_{\text{dd}}(^{164}\text{Er})\approx a_{\text{dd}}(^{166}\text{Er})\approx 65a_0$ , where  $a_0$  is the Bohr radius. In each of the two components  $a > a_{\text{dd}}$ , which stops the binding of solitons in each component in isolation, whereas a binary quasi-1D or a quasi-2D  $^{164}\text{Er}$ - $^{166}\text{Er}$  soliton is bound in the presence of an interspecies dipolar interaction. The stationary states were obtained by imaginary-time propagation of the underlying mean-field model; dynamical stability of the solitons was established by real-time propagation over a long period of time.

## I. INTRODUCTION

A soliton [1, 2] is a self-reinforcing localized stable wave packet, which is bound due to a cancellation of nonlinear attraction and linear repulsion. A soliton preserves its shape, while propagating at a constant velocity, and also after collisions with other such localized wave packets. Solitons have been created and studied in a  $^7\text{Li}$  [3, 4] and  $^{85}\text{Rb}$  [5] Bose-Einstein condensate (BEC) by tuning the atomic scattering length to a desired negative value by varying an external electromagnetic field near a Feshbach resonance [6], so that the nonlinear attraction becomes equal to the linear repulsion. A binary soliton is a solitary wave with two components that maintains its shape during propagation. Most of the binary solitons in a BEC are self attractive and bound basically by intraspecies attraction, independent of the nature of the interspecies interaction: attractive or repulsive. A symbiotic soliton in a binary BEC [7, 8] necessarily has a repulsive intraspecies interaction and is bound due to an attractive interspecies interaction. Each component of such a symbiotic soliton cannot be bound in isolation and the presence of the second component is essential for its formation. There have been studies of a symbiotic gap soliton [9, 10], of the dynamics of a symbiotic soliton [11], and of a two-dimensional (2D) symbiotic soliton [12–14]. Although a quasi-one-dimensional (quasi-1D) soliton can be stabilized in a self-attractive BEC in the presence of an attractive contact interaction alone [15], a quasi-2D or a three-dimensional (3D) soliton cannot be stabilized in a BEC by contact interaction alone, due to a collapse instability [1, 16, 17]. However, a quasi-2D or a 3D soliton can be stabilized by some other interaction e.g., in the presence of a long-range dipolar interaction [18, 19]

in two dimensions [20] and in the presence of a spin-orbit coupling interaction [21] in one [22], two [23–25] and three [26] dimensions. In fact, 2D solitons are possible [27, 28] in a general class of nonlinear nonlocal systems and a dipolar BEC is a special type of such a system which can stabilize a quasi-2D soliton. There have been many studies of solitons in dipolar BECs under different conditions [29–32]. In a three-component BEC and in a spin-orbit coupled hyperfine spin-1 BEC, it is also possible to have a symbiotic soliton [14]. In the latter case, in addition to a symbiotic soliton in 1D, it is also possible to have such a soliton in 2D.

An anisotropic quasi-2D soliton [20] mobile in the  $x$ - $z$  plane containing the polarization  $z$  direction, can be created in a dipolar BEC for  $a < a_{\text{dd}}$ , while the dipolar interaction dominates over the contact interaction, where  $a$  is the atomic scattering length and  $a_{\text{dd}}$  is the dipolar length [defined by Eq. (4) below]. In addition, there could be a quasi-1D dipolar soliton [15] mobile along the  $z$  [33] or  $x$  [34] direction. The quasi-2D soliton is anisotropic in the  $x$ - $z$  plane (elongated along the  $z$  direction) due to the action of the anisotropic dipolar interaction. In the opposite extreme, while  $a > a_{\text{dd}}$ , the net interaction is repulsive and no quasi-1D or quasi-2D soliton can be formed in such a self-repulsive dipolar BEC. Similarly, in a binary dipolar BEC, for  $a > a_{\text{dd}}$  in each component, no soliton can be realized in each component in isolation. As the anisotropic long-range nonlocal dipolar interaction is partly attractive and partly repulsive, and is hence basically different from an isotropic contact interaction, it would be interesting to see if the interspecies dipolar interaction alone can stabilize a symbiotic dipolar soliton. The net attraction due to dipolar interaction increases as the net interspecies dipole moment of the binary soliton increases and that happens as the number of atoms increases for a fixed atomic dipole moment, viz. Fig. 3 and Fig. 5.

In this paper we demonstrate, in the presence of a suffi-

\*sk.adhikari@unesp.br, <https://professores.ift.unesp.br/sk.adhikari>

ciently strong interspecies dipolar interaction and zero interspecies contact interaction, the formation of a different type of symbiotic soliton in a binary dipolar BEC with net repulsive intraspecies interaction, where each component cannot be bound in isolation and the binding comes from the interspecies dipolar interaction. It is well known that an attractive interspecies contact interaction can bind a symbiotic soliton [7, 8]. We will set the interspecies contact interaction to zero, so that the effect of the interspecies dipolar interaction on the formation of the bound soliton can be studied. We consider a binary dipolar BEC in the  $^{164}\text{Er}$ - $^{166}\text{Er}$  mixture with experimental scattering lengths [35]  $a(^{164}\text{Er})=81a_0$  and  $a(^{166}\text{Er})=68a_0$  and with dipolar lengths  $a_{\text{dd}}(^{164}\text{Er})\approx a_{\text{dd}}(^{166}\text{Er})\approx 65a_0$ , where  $a_0$  is the Bohr radius. In this system, for each of the components  $a > a_{\text{dd}}$ , and, because of the dominance of the repulsive contact interaction, no soliton can be created in each component in isolation, although a quasi-1D as well as a quasi-2D symbiotic dipolar soliton may exist for an adequate interspecies dipolar interaction and a zero interspecies contact interaction. In this study, we use a numerical solution of the mean-field Gross-Pitaevskii (GP) equation [36, 37], by imaginary- and real-time propagation, including an intraspecies and interspecies dipolar and contact interactions [18] in reduced dimensions [19, 38].

In Sec. II we present the quasi-1D and quasi-2D mean-field models relevant for this study. In Sec. IIA we present the mean-field 3D GP equation [18, 19] for a binary dipolar BEC. In Sec. IIB, following Refs. [39, 40], we present a derivation of the mean-field equation for a quasi-2D binary dipolar BEC in the  $x$ - $z$  plane, with a strong trap along the  $y$  direction, by integrating out the  $y$  variable, which will be used to study a quasi-2D symbiotic dipolar soliton. The mean-field equation for a quasi-1D binary dipolar BEC [41] along the  $z$  direction with a strong trap in the  $x$ - $y$  plane is then derived in Sec. IIC by integrating out the  $x$  and  $y$  variables in the 3D mean-field model. We use these quasi-1D and quasi-2D models to study symbiotic quasi-1D and quasi-2D dipolar BEC solitons, respectively. In Sec. III A 1 (III A 2) we present numerical results of phase plot and density for the formation of a quasi-1D (quasi-2D) symbiotic dipolar soliton employing an imaginary-time propagation of the relevant mean-field model. In Sec. IIIB we establish the dynamical stability of these solitons using a real-time propagation of these models after inflicting a small perturbation, employing the converged imaginary-time solution as the initial state. Finally, in Sec. IV we present a summary of our findings.

## II. MEAN-FIELD MODEL

### A. Three-dimensional model

We consider a binary BEC of dipolar atoms, with the mass, magnetic dipole moment, number of atoms and

intraspecies scattering length denoted by  $m_i, \mu_i, N_i, a_i$ , respectively, with  $i = 1, 2$  for the two species. All dipolar atoms have their dipolar moments polarized along the  $z$  direction. The interspecies scattering length of the two types of atom is  $a_{12}$ . The intraspecies and interspecies interactions are given by [18, 42]

$$V_i(\mathbf{R}) = \frac{\mu_0 \mu_i^2}{4\pi} U_{\text{dd}}(\mathbf{R}) + \frac{4\pi \hbar^2 a_i}{m} \delta(\mathbf{R}), \quad (1)$$

$$V_{12}(\mathbf{R}) = \frac{\mu_0 \mu_1 \mu_2}{4\pi} U_{\text{dd}}(\mathbf{R}) + \frac{2\pi \hbar^2 a_{12}}{m_R} \delta(\mathbf{R}), \quad (2)$$

$$U_{\text{dd}}(\mathbf{R}) = \frac{1 - 3 \cos^2 \theta}{|\mathbf{R}|^3}, \quad (3)$$

where  $m_R = (m_1 + m_2)/(m_1 m_2)$  is the reduced mass of the two types of atoms,  $\mu_0$  is the permeability of vacuum,  $\mathbf{R} = \mathbf{r} - \mathbf{r}'$  is the vector joining two dipoles placed at  $\mathbf{r} \equiv \{x, y, z\}$  and  $\mathbf{r}' \equiv \{x', y', z'\}$  and  $\theta$  is the angle made by  $\mathbf{R}$  with the  $z$  axis. The strength of dipolar interaction is given by the following intraspecies ( $a_{\text{dd}}^{(i)}$ ) and interspecies ( $a_{\text{dd}}^{(12)}$ ) dipolar lengths

$$a_{\text{dd}}^{(i)} = \frac{\mu_0 \mu_i^2 m_i}{12\pi \hbar^2}, \quad a_{\text{dd}}^{(12)} = \frac{\mu_0 \mu_1 \mu_2 m_R}{6\pi \hbar^2}. \quad (4)$$

The binary dipolar BEC is described by the following nonlocal nonlinear 3D mean-field GP equation [18, 42]

$$\begin{aligned} i\hbar \frac{\partial \psi_i(\mathbf{r}, t)}{\partial t} = & \left[ -\frac{\hbar^2}{2m_i} \nabla_{\mathbf{r}}^2 + V_i(\mathbf{r}) + \frac{4\pi \hbar^2}{m_i} a_i N_i |\psi_i(\mathbf{r}, t)|^2 \right. \\ & + \frac{3\hbar^2}{m_i} a_{\text{dd}}^{(i)} N_i \int U_{\text{dd}}(\mathbf{R}) |\psi_i(\mathbf{r}', t)|^2 d\mathbf{r}' \\ & + \frac{2\pi \hbar^2}{m_R} a_{12} N_j |\psi_j(\mathbf{r}, t)|^2 \\ & \left. + \frac{3\hbar^2}{2m_R} a_{\text{dd}}^{(12)} N_j \int U_{\text{dd}}(\mathbf{R}) |\psi_j(\mathbf{r}', t)|^2 d\mathbf{r}' \right] \psi_i(\mathbf{r}, t), \quad (5) \end{aligned}$$

where  $i \neq j$ ,  $i, j = 1, 2$ ,  $\nabla_{\mathbf{r}}^2 = (\partial^2/\partial x^2 + \partial^2/\partial y^2 + \partial^2/\partial z^2)$ ,  $V_i(\mathbf{r}) = \frac{1}{2} m_i (\omega_x^2 x^2 + \omega_y^2 y^2 + \omega_z^2 z^2)$  is the confining trap with angular frequencies  $\omega_x, \omega_y, \omega_z$  along  $x, y, z$  directions, respectively. The wave function is normalized as  $\int |\psi_i(\mathbf{r}, t)|^2 d\mathbf{r} = 1$ .

Equation (5) can be reduced to the following dimensionless form by scaling lengths in units of  $l = \sqrt{\hbar/m\omega_0}$ , time in units of  $\omega_0^{-1}$ , angular frequencies  $\omega_x, \omega_y, \omega_z$  in units of  $\omega_0$ , energy in units of  $\hbar\omega_0$ , and density  $|\psi_i|^2$  in units of  $l^{-3}$ , where  $\omega_0$  is a reference frequency

$$\begin{aligned} i \frac{\partial \psi_1(\mathbf{r}, t)}{\partial t} = & \left[ -\frac{1}{2} \nabla_{\mathbf{r}}^2 + V_1(\mathbf{r}) + g_1 |\psi_1(\mathbf{r}, t)|^2 \right. \\ & + g_{\text{dd}}^{(1)} \int U_{\text{dd}}(\mathbf{R}) |\psi_1(\mathbf{r}', t)|^2 d\mathbf{r}' + g_{12} |\psi_2(\mathbf{r}, t)|^2 \\ & \left. + g_{\text{dd}}^{(12)} \int U_{\text{dd}}(\mathbf{R}) |\psi_2(\mathbf{r}', t)|^2 d\mathbf{r}' \right] \psi_1(\mathbf{r}, t), \quad (6) \end{aligned}$$

$$\begin{aligned}
i \frac{\partial \psi_2(\mathbf{r}, t)}{\partial t} = & \left[ -\frac{m_{12}}{2} \nabla_{\mathbf{r}}^2 + V_2(\mathbf{r}) + g_2 |\psi_2(\mathbf{r}, t)|^2 \right. \\
& + g_{\text{dd}}^{(2)} \int U_{\text{dd}}(\mathbf{R}) |\psi_2(\mathbf{r}', t)|^2 d\mathbf{r}' + g_{21} |\psi_1(\mathbf{r}, t)|^2 \\
& \left. + g_{\text{dd}}^{(21)} \int U_{\text{dd}}(\mathbf{R}) |\psi_1(\mathbf{r}', t)|^2 d\mathbf{r}' \right] \psi_2(\mathbf{r}, t), \quad (7)
\end{aligned}$$

where  $V_1(\mathbf{r}) = \frac{1}{2}(\omega_x^2 x^2 + \omega_y^2 y^2 + \omega_z^2 z^2)$  and  $V_2(\mathbf{r}) = \frac{1}{2m_{12}}(\omega_x^2 x^2 + \omega_y^2 y^2 + \omega_z^2 z^2)$ ,  $m_{12} = m_1/m_2$ ,  $g_1 = 4\pi N_1 a_1$ ,  $g_2 = 4\pi a_2 N_2 m_{12}$ ,  $g_{12} = 2\pi m_1 a_{12} N_2/m_R$ ,  $g_{21} = 2\pi m_1 a_{12} N_1/m_R$ ,  $g_{\text{dd}}^{(1)} = 3N_1 a_{\text{dd}}^{(1)}$ ,  $g_{\text{dd}}^{(2)} = 3N_2 a_{\text{dd}}^{(2)} m_{12}$ ,  $g_{\text{dd}}^{12} = 3N_2 a_{\text{dd}}^{12} m_1/2m_R$ ,  $g_{\text{dd}}^{21} = 3N_1 a_{\text{dd}}^{12} m_1/2m_R$ . Here we are using, without any risk of confusion, the same symbols to represent the scaled (dimensionless) and unscaled variables and in Eqs. (6) and (7) and in the following equations all variables are dimensionless. Equations (6) and (7) can also be obtained from the variational rule [43]

$$i \frac{\partial \psi_i}{\partial t} = \frac{\delta E}{\delta \psi_i^*} \quad (8)$$

with the following energy functional (total energy)

$$\begin{aligned}
E = & \frac{1}{2} \int d\mathbf{r} \left[ N_1 |\nabla_{\mathbf{r}} \psi_1(\mathbf{r})|^2 + N_2 m_{12} |\nabla_{\mathbf{r}} \psi_2(\mathbf{r})|^2 \right. \\
& + \sum_{i=1}^2 \left\{ 2N_i V_i |\psi_i(\mathbf{r})|^2 + N_i g_i |\psi_i(\mathbf{r})|^4 \right. \\
& \left. + N_i g_{\text{dd}}^{(i)} |\psi_i(\mathbf{r})|^2 \int U_{\text{dd}}(\mathbf{R}) |\psi_i(\mathbf{r}')|^2 d\mathbf{r}' \right\} \\
& + 2N_1 g_{12} |\psi_1(\mathbf{r})|^2 |\psi_2(\mathbf{r})|^2 \\
& \left. + 2N_1 g_{\text{dd}}^{(12)} |\psi_1(\mathbf{r})|^2 \int U_{\text{dd}}(\mathbf{R}) |\psi_2(\mathbf{r}')|^2 d\mathbf{r}' \right] \quad (9)
\end{aligned}$$

for a stationary state.

## B. Quasi-2D reduction

First we present the effective quasi-2D equations under a strong trap along the  $y$  direction, perpendicular to the polarization  $z$  direction, while the binary dipolar condensate remain mostly confined in the  $x$ - $z$  plane with a much smaller spatial extension along the  $y$  direction. Because of the anisotropic dipolar interaction, the profile of the binary condensate in the  $x$ - $z$  plane is circularly asymmetric. In this case, we have  $\omega_y \gg \omega_\rho \equiv \omega_x = \omega_z$ , and the dipolar BEC is assumed to be in the stationary ground state  $\phi_i(y) = e^{-y^2/2d_{y(i)}^2}/(\pi d_{y(i)}^2)^{1/4}$  of the axial trap and the 3D wave function  $\psi_i(\mathbf{r}, t)$  can be written as [39, 40]

$$\psi_i(\mathbf{r}, t) \equiv \phi_i(y) \times \psi_{2\text{D}}^{(i)}(\boldsymbol{\rho}, t) = \frac{e^{-\frac{y^2}{2d_{y(i)}^2}}}{(\pi d_{y(i)}^2)^{1/4}} \psi_{2\text{D}}^{(i)}(\boldsymbol{\rho}, t), \quad (10)$$

where  $\boldsymbol{\rho} \equiv \{x, z\}$ ,  $\mathbf{r} \equiv \{\boldsymbol{\rho}, y\}$ ,  $\psi_{2\text{D}}^{(i)}(\boldsymbol{\rho}, t)$  is the effective quasi-2D wave function and the axial harmonic oscillator lengths  $d_{y(1)} = \sqrt{1/\omega_y}$  and  $d_{y(2)} = \sqrt{m_{12}/\omega_y}$ . Equation (10) implies that the wave function is frozen in the ground state  $\phi_i(y)$  in the  $y$  direction, and the essential dynamics is governed by the wave function  $\psi_{2\text{D}}^{(i)}(\boldsymbol{\rho}, t)$  in the  $x$ - $z$  plane. The quasi-2D wave function in Eq. (10) is normalized as  $\int |\psi_{2\text{D}}^{(i)}(\boldsymbol{\rho}, t)|^2 d\boldsymbol{\rho} = 1$ .

Using ansatz (10) in Eqs. (6) and (7), the  $y$  dependence can be integrated out to obtain the following effective quasi-2D equation [39, 40]

$$\begin{aligned}
i \frac{\partial \psi_{2\text{D}}^{(i)}(\boldsymbol{\rho}, t)}{\partial t} = & \left[ -\frac{\nabla_{\boldsymbol{\rho}}^2}{2} + c_i N_i |\psi_{2\text{D}}^{(i)}(\boldsymbol{\rho}, t)|^2 \right. \\
& + c_{12} N_j |\psi_{2\text{D}}^{(j)}(\boldsymbol{\rho}, t)|^2 + c_{\text{dd}}^{(i)} N_i C_{2\text{D}}^{(i)}(\boldsymbol{\rho}, t) \\
& \left. + c_{\text{dd}}^{(12)} N_j C_{2\text{D}}^{(j)}(\boldsymbol{\rho}, t) \right] \psi_{2\text{D}}^{(i)}(\boldsymbol{\rho}, t), \quad (11)
\end{aligned}$$

where  $i, j = 1, 2$ ,  $i \neq j$ ,  $\nabla_{\boldsymbol{\rho}}^2 \equiv (\partial^2/\partial x^2 + \partial^2/\partial z^2)$ ,  $c_i = 4\pi a_i/(\sqrt{2\pi}d_y)$ ,  $c_{12} = 4\pi a_{12}/(\sqrt{2\pi}d_y)$ ,  $c_{\text{dd}}^{(i)} = 4\pi a_{\text{dd}}^{(i)}/(\sqrt{2\pi}d_y)$ ,  $c_{\text{dd}}^{(12)} = 4\pi a_{\text{dd}}^{(12)}/(\sqrt{2\pi}d_y)$ , and, without any loss of generality, we have taken the mass of the two components to be equal in Eq. (11) ( $m_1 = m_2, m_{12} = 1, d_{y(1)} = d_{y(2)} = \sqrt{1/\omega_y}$ ) and the same intraspecies and interspecies dipolar lengths for the two components. This will be achieved by considering two nearby isotopes of the same atom in the binary mixture. Consequently, in the present study,  $a_{\text{dd}}^{(12)} \approx a_{\text{dd}}^{(1)} \approx a_{\text{dd}}^{(2)}$ . However, the scattering lengths remain different  $a_{12} \neq a_1 \neq a_2$ . The equal-mass condition on the components has allowed us to write the quasi-2D binary equation in the compact form (11). As we will study the problem of a symbiotic binary vector soliton, we have set the trapping potential in Eq. (11) to zero. The nonlinear nonlocal dipolar term  $C_{2\text{D}}^{(i)}(\boldsymbol{\rho}, t)$ , containing the effective nonlocal dipolar interaction  $U_{\text{dd}}^{2\text{D}}(|\boldsymbol{\rho} - \boldsymbol{\rho}'|)$ , is evaluated, after a Fourier transformation to the momentum ( $k$ ) space, as [39, 40]

$$C_{2\text{D}}^{(i)}(\boldsymbol{\rho}, t) \equiv \int U_{\text{dd}}^{2\text{D}}(|\boldsymbol{\rho} - \boldsymbol{\rho}'|) n_i(\boldsymbol{\rho}', t) d\boldsymbol{\rho}', \quad (12)$$

$$= \int \frac{d^2 k_\rho}{(2\pi)^2} e^{i\mathbf{k}_\rho \cdot \boldsymbol{\rho}} \tilde{n}_i(\mathbf{k}_\rho, t) f_{2\text{D}}\left(\frac{k_\rho d_y}{\sqrt{2}}\right), \quad (13)$$

$$\tilde{n}_i(\mathbf{k}_\rho, t) = \int e^{i\mathbf{k}_\rho \cdot \boldsymbol{\rho}} n_i(\boldsymbol{\rho}, t) d\boldsymbol{\rho}, \quad (14)$$

$$f_{2\text{D}}(\xi) = \frac{1}{\sqrt{2\pi}d_y} [-1 + 3\sqrt{\pi} \frac{\xi_z^2}{\xi} e^{\xi^2} \{1 - \text{erf } \xi\}], \quad (15)$$

$$\text{erf } \xi = \frac{2}{\sqrt{\pi}} \int_0^\xi e^{-u^2} du \quad (16)$$

where normalized density  $n_i(\boldsymbol{\rho}, t) = |\psi_{2\text{D}}^{(i)}(\boldsymbol{\rho}, t)|^2$ ,  $\xi = k_\rho d_y/\sqrt{2}$ ,  $\xi_z = k_z d_y/\sqrt{2}$ , erf is the error function,  $\mathbf{k}_\rho \equiv \{k_x, k_z\}$ .

The effective total energy of the system for a quasi-2D

stationary state is

$$E = \int d\rho \frac{1}{2} \sum_i \left[ N_i |\nabla_\rho \psi_{2D}^{(i)}(\rho)|^2 + c_i N_i^2 |\psi_{2D}^{(i)}(\rho)|^4 \right. \\ \left. + c_{dd}^{(i)} N_i^2 C_{2D}^{(i)}(\rho) |\psi_{2D}^{(i)}(\rho)|^2 \right] + \int d\rho N_1 N_2 |\psi_{2D}^{(2)}(\rho)|^2 \\ \times \left[ c_{dd}^{(12)} C_{2D}^{(1)}(\rho) + c_{12} |\psi_{2D}^{(1)}(\rho)|^2 \right]. \quad (17)$$

For the study of quasi-2D soliton the harmonic trap frequency  $\omega_\rho$  has been set equal to 0 in Eqs. (11) and (17).

### C. Quasi-1D reduction

We consider a binary dipolar BEC with a strong trap in the  $x$ - $y$  plane, while the dipolar condensate remain elongated along the polarization  $z$  direction with a relatively small radius in the  $x$ - $y$  plane. In this case, we take  $\omega_x = \omega_y = \omega_\rho \gg \omega_z$ , and we assume that in the radial direction the dipolar BEC is confined in the stationary ground state  $\phi_i(\rho) = e^{-\rho^2/2d_{\rho(i)}^2}/(d_{\rho(i)}\sqrt{\pi})$  of the transverse trap. Consequently, the wave function  $\psi_i(\mathbf{r})$  can be written as [41]

$$\psi_i(\mathbf{r}, t) \equiv \phi_i(\rho) \times \psi_{1D}^{(i)}(z, t) = \frac{e^{-\frac{\rho^2}{2d_{\rho(i)}^2}}}{\sqrt{\pi d_{\rho(i)}^2}} \psi_{1D}^{(i)}(z, t), \quad (18)$$

where  $\psi_{1D}^{(i)}(z, t)$  is the effective quasi-1D wave function and  $d_{\rho(i)} = 1/\sqrt{\omega_\rho}$  is the radial harmonic oscillator length. As in the quasi-2D case, we are again assuming equal mass for the atoms of the two components:  $m_1 = m_2, m_{12} = 1, d_{\rho(1)} = d_{\rho(2)}$ . Equation (18) implies that the wave function is frozen in the ground state  $\phi_i(\rho)$  in the  $x$ - $y$  plane, and the essential dynamics is confined along the polarization  $z$  direction governed by the quasi-1D wave function  $\psi_{1D}^{(i)}(z, t)$ . The wave function in Eq. (18) is normalized as  $\int_{-\infty}^{\infty} |\psi_{1D}^{(i)}(z, t)|^2 dz = 1$ .

Using ansatz (18) in Eqs. (6) and (7), the  $x, y$  dependence can be integrated out to obtain the following effective quasi-1D equation [41]

$$i \frac{\partial \psi_{1D}^{(i)}(z, t)}{\partial t} = \left[ -\frac{1}{2} \frac{\partial^2}{\partial z^2} + h_i N_i |\psi_{1D}^{(i)}(z, t)|^2 \right. \\ \left. + h_{12} N_j |\psi_{1D}^{(j)}(z, t)|^2 + h_{dd}^{(i)} N_i C_{1D}^{(i)}(z, t) \right. \\ \left. + h_{dd}^{(12)} N_j C_{1D}^{(j)}(z, t) \right] \psi_{1D}^{(i)}(z, t), \quad (19)$$

where  $h_i = 2a_i/d_\rho^2$ ,  $h_{12} = 2a_{12}/d_\rho^2$ ,  $h_{dd}^{(i)} = 2a_{dd}^{(i)}/d_\rho^2$ ,  $h_{dd}^{(12)} = 2a_{dd}^{(12)}/d_\rho^2$ , where the nonlinear nonlocal dipolar term

$$C_{1D}^{(i)}(z, t) \equiv \int_{-\infty}^{\infty} U_{dd}^{1D}(|z - z'|) n_i(z', t) dz', \quad (20)$$

where density  $n_i(z, t) \equiv |\psi_{1D}^{(i)}(z, t)|^2$  and the effective nonlocal dipolar interaction  $U_{dd}^{1D}(|z - z'|)$ , is evaluated, after a Fourier transformation to the momentum ( $k$ ) space, as

$$C_{1D}^{(i)}(z, t) \equiv \int_{-\infty}^{\infty} \frac{dk_z}{2\pi} e^{ik_z z} \tilde{n}_i(k_z, t) s_{1D} \left( \frac{k_z d_\rho}{\sqrt{2}} \right), \quad (21)$$

$$s_{1D}(\zeta) = \int_0^\infty du \left[ \frac{3\zeta^2}{u + \zeta^2} - 1 \right] e^{-u}, \quad (22)$$

$$\tilde{n}_i(k_z, t) = \int_{-\infty}^{\infty} e^{ik_z z} n_i(z, t) dz. \quad (23)$$

The effective total energy of the system for a stationary state is

$$E = \int_{-\infty}^{\infty} dz \frac{1}{2} \sum_i \left[ N_i |\partial_z \psi_{1D}^{(i)}(z)|^2 + h_i N_i^2 |\psi_{1D}^{(i)}(z)|^4 \right. \\ \left. + h_{dd}^{(i)} N_i^2 C_{1D}^{(i)}(z) |\psi_{1D}^{(i)}(z)|^2 \right] + \int_{-\infty}^{\infty} dz N_1 N_2 |\psi_{1D}^{(2)}(z)|^2 \\ \times \left[ h_{dd}^{(12)} C_{1D}^{(1)}(z) + h_{12} |\psi_{1D}^{(1)}(z)|^2 \right]. \quad (24)$$

For the study of quasi-1D soliton the harmonic trap frequency  $\omega_z$  has been set equal to 0 in Eqs. (19) and (24).

## III. RESULT AND DISCUSSION

We numerically solve the partial differential GP equations using the split-time-step Crank-Nicolson method [44] by imaginary- and real-time propagation. For a numerical simulation there are the FORTRAN [44] and C [19] programs for the solution of the GP equation and their open-multiprocessing [45, 46] version appropriate for dipolar BEC. The imaginary-time method was used to find the stationary ground states of the solitons. The real-time propagation method was used to study the dynamics with the converged solution obtained by imaginary-time propagation as the initial state. The space steps employed for the solution of Eqs. (11) and (19) to obtain the quasi-2D and quasi-1D symbiotic solitons by the imaginary-time propagation are  $dz = dx = 0.1$  and  $dz = 0.1$ , respectively, and the corresponding time steps are  $dt = 0.1dzdx$  and  $dt = 0.1dz^2$ , respectively; in real-time propagation the corresponding time steps were  $dt = 0.05dzdx$  and  $dt = 0.05dz^2$ , respectively.

In this demonstration of a quasi-1D and quasi-2D symbiotic dipolar soliton, we consider a binary dipolar mixture, where naturally there cannot be a soliton in each component in isolation; and this happens for  $a_i > a_{dd}^{(i)}$ , while the net intraspecies interaction in each component is repulsive. For this purpose we consider a dipolar  $^{166}\text{Er}$ - $^{164}\text{Er}$  mixture where  $a_{dd}^{(1)} \equiv a_{dd}^{(166}\text{Er}) \approx a_{dd}^{(2)} \equiv a_{dd}^{(164}\text{Er}) \approx 65a_0 \approx a_{dd}^{(12)}$  corresponding to a dipole moment  $\mu = 7\mu_B$ , where  $\mu_B$  is a Bohr magneton and the experimental values of the scattering lengths are [35]  $a^{(1)} \equiv a^{(166}\text{Er}) = 68a_0$ ,  $a^{(2)} \equiv a^{(164}\text{Er}) = 81a_0$ ,

so that  $a_i > a_{\text{dd}}^{(i)}$  for each of these components and no soliton can be formed in each component in isolation in the absence of any interspecies interaction. In this study we take the scaling length  $l = \sqrt{\hbar/m\omega_0} = 1 \mu\text{m}$ , corresponding to a reference frequency  $\omega_0 = 2\pi \times 61.26 \text{ Hz}$  for  $m = 165 \text{ amu}$ , the quasi-2D axial harmonic oscillator length in dimensionless units  $d_y = 1/\sqrt{3}$ , and the quasi-1D radial harmonic oscillator length  $d_\rho = 1/2$ . These lengths provide a scaling of the problem and should not change the conclusions of this study.

It is well-known that a symbiotic binary soliton can be bound by an attractive interspecies contact interaction [7, 8]. In this study, we demonstrate that such a symbiotic soliton can be bound by an interspecies long-range dipolar interaction and investigate its properties. Here we emphasize the effect of interspecies dipolar interaction alone on the formation and dynamics of such a soliton. Hence, we will take the interspecies scattering length  $a_{12} = 0$  in the study of stationary solitons in Sec. III A. In the demonstration of dynamical stability, a small negative value will be attributed to  $a_{12}$  in Sec. III B. Once the interspecies dipolar interaction is switched on, maintaining the interspecies contact interaction zero ( $a_{12} = 0$ ), a quasi-1D or quasi-2D binary symbiotic dipolar soliton can be formed. The interspecies contact interaction can be kept negligibly small by manipulating an external electromagnetic field near a Feshbach resonance [6]. Besides this, all other interaction parameters – scattering lengths and dipolar lengths – are fixed at their known experimental values [35]. In this study, the only approximation is taking the masses of the isotopes  $^{166}\text{Er}$  and  $^{164}\text{Er}$  to be equal to 165 atomic units. This greatly simplifies the book keeping without any consequence on our findings.

## A. Stationary soliton

### 1. Quasi-1D symbiotic dipolar soliton

The profile of a quasi-1D dipolar condensate is illustrated in Fig. 1(a). Due to the strong trap in the  $x$ - $y$  plane the condensate is elongated along the polarization  $z$  direction with a circular section in the  $x$ - $y$  plane. In the quasi-1D model the solitons are strictly one-dimensional and lie along the  $z$  axis. The formation of a quasi-1D symbiotic dipolar soliton in the  $^{166}\text{Er}$ - $^{164}\text{Er}$  mixture is illustrated in the energy versus  $N_1$  phase plot for different  $N_2$  displayed in Fig. 2. We find that, for  $N_2 = N_1$ , the binding energy of the soliton increases linearly with the number of atoms. There is no collapse in this quasi-1D case [1]; the binding energy does not diverge for a finite number of atoms for any set of parameters. From the expression for total energy given by Eq. (24), we realize that the linear dependence of Fig. 2 would be possible, if the component wave functions  $\psi_{1\text{D}}^{(i)}$  were independent of the number of atoms ( $N_1 = N_2$ ) and if the deriva-

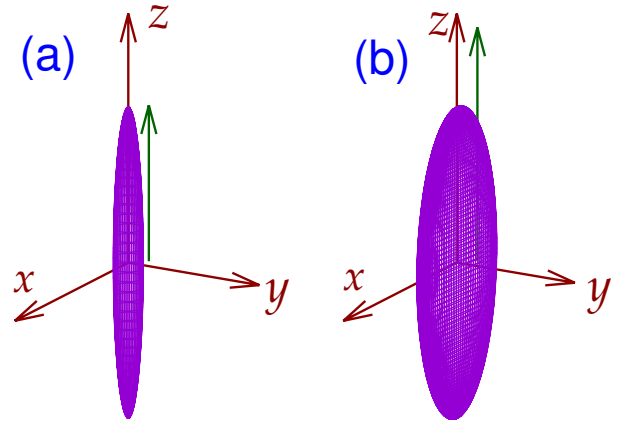


FIG. 1: (Color online) Profile of a (a) quasi-1D and a (b) quasi-2D dipolar BEC condensate. The green arrow represents the direction of dipole moment of an atom. In (a) we have a strong trap in the  $x$ - $y$  plane and the condensate is mostly aligned along the polarization  $z$  direction with a circular profile of small radius in the  $x$ - $y$  plane. In (b) we have a strong trap along the  $y$  direction and the condensate mostly lies in the  $x$ - $z$  plane with a small width in the  $y$  direction. Due to the anisotropic dipolar interaction the section in the  $x$ - $z$  plane is always elongated in the  $z$  direction.

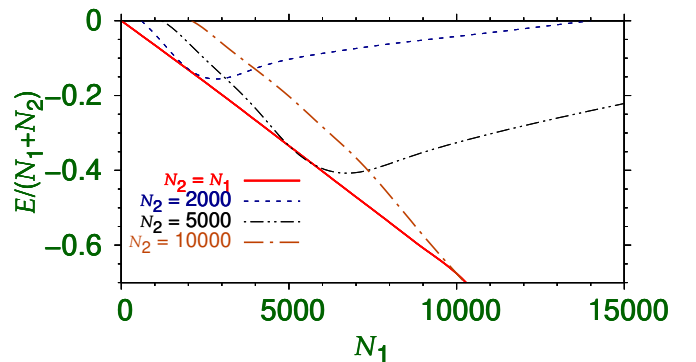


FIG. 2: (Color online) Phase diagram showing the effective energy per atom  $[E/(N_1+N_2)]$  of a quasi-1D symbiotic soliton in the  $^{166}\text{Er}$ - $^{164}\text{Er}$  mixture versus the number of atoms  $N_1$  for different  $N_2 = N_1, 2000, 5000$  and  $10000$ , where (throughout this paper) the first component denoted  $i = 1$  is  $^{166}\text{Er}$  and the second component ( $i = 2$ ) is  $^{164}\text{Er}$ . The parameters for the  $^{166}\text{Er}$ - $^{164}\text{Er}$  mixture, used in this paper are,  $a_1 = a(^{166}\text{Er}) = 68a_0$ ,  $a_2 = a(^{164}\text{Er}) = 81a_0$ ,  $a_{12} = a(^{166}\text{Er}-^{164}\text{Er}) = 0$ ,  $a_{\text{dd}}(^{166}\text{Er}) \approx a_{\text{dd}}(^{164}\text{Er}) \approx 65a_0$ ; the scaling length  $l = 1 \mu\text{m}$  and quasi-1D radial harmonic oscillator length  $d_\rho = 1/2$ . All quantities in this and following figures are dimensionless.

tive term  $|\partial_z \psi_{1\text{D}}^{(i)}(z)|^2$  in that equation contributes to a negligibly small amount in this Thomas-Fermi limit [19] of large number of dipolar atoms. Then after neglecting the derivative term in Eq. (24), we find that, for  $N_1 = N_2 = N$ , the quantity  $N^2$  scales out of Eq. (24) and we have  $E \propto N^2$ ; consequently  $E/N \propto N$ , consistent

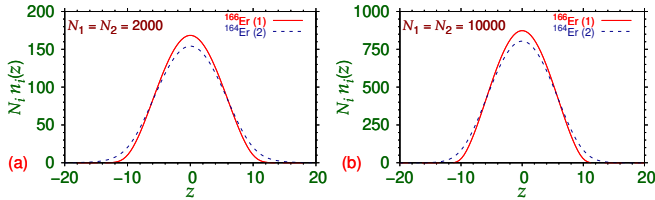


FIG. 3: (Color online) Dimensionless linear density  $N_i n_i(z) \equiv N_i |\psi_{1D}^{(i)}(z)|^2$ , with normalization  $\int_{-\infty}^{\infty} N_i n_i(z) dz = N_i$ , of a quasi-1D symbiotic soliton in a binary dipolar BEC of the  $^{166}\text{Er}$ - $^{164}\text{Er}$  mixture for (a)  $N_1 = N_2 = 2000$  and (b)  $N_1 = N_2 = 10000$ .

with the linear dependence in Fig. 2. For  $N_1 \neq N_2$  no such simple dependence of energy is found in Fig. 2. For  $N_1 \neq N_2$ , for a fixed  $N_2$ , the binding energy per atom increases for small  $N_1$ ; but for large  $N_1$  ( $\gg N_2$ ), the net intraspecies repulsion in component  $i = 1$  ( $^{166}\text{Er}$ ) increases more rapidly than the increase of the interspecies attraction, thus causing a decrease in the binding energy per atom with the increase of  $N_1$  in Fig. 2 as found for  $N_2 = 2000$  and  $5000$ . The same behavior exists for  $N_2 = 10000$  and for  $N_1 > 10000$  (not considered here).

In Fig. 3 we exhibit the linear densities  $N_i n_i(z)$  versus  $z$  of the two components ( $i = 1, 2$ ) of the quasi-1D symbiotic dipolar soliton in the  $^{166}\text{Er}$ - $^{164}\text{Er}$  mixture for (a)  $N_1 = N_2 = 2000$  and (b)  $N_1 = N_2 = 10000$ . Because of the quasi-symmetry of the two components, the normalized densities,  $n_i(z)$ ,  $N \equiv N_1 = N_2$ , [ $\int_{-\infty}^{\infty} dz n_i(z) = 1$ ] of the two components are practically the same in both cases. Moreover, these densities [ $n_i(z)$ ] for  $N_1 = N_2 = 2000$  and  $N_1 = N_2 = 10000$  are also very similar [although the real densities  $N_i n_i(z)$  are proportional to the number of atoms and are different], which was conjectured from the linear dependence of energy in Fig. 2 for  $N_1 = N_2$ . The very similar normalized densities of the two components in Figs. 3(a)-(b), for large number of atoms in the Thomas-Fermi limit, lead to the linear dependence of energy in Fig. 2 for  $N_1 = N_2$ .

In Fig. 4 we exhibit the linear densities  $N_i n_i(z)$  versus  $z$  of the two components ( $i = 1, 2$ ) of the quasi-1D symbiotic dipolar soliton in the  $^{166}\text{Er}$ - $^{164}\text{Er}$  mixture for (a)  $N_1 = 10000, N_2 = 5000$ , (b)  $N_1 = 4000, N_2 = 2000$ , (c)  $N_1 = 3000, N_2 = 5000$ , and (d)  $N_1 = 7000, N_2 = 10000$ , where the symmetry between the two components is broken due to a different number of atoms in the two components ( $N_1 \neq N_2$ ). Consequently, the densities for  $N_1 > N_2$  are distinct from those for  $N_1 < N_2$  as found by comparing Figs. 4(a)-(b) for  $N_1 > N_2$  with Figs. 4(c)-(d) for  $N_1 < N_2$ . These densities for  $N_1 \neq N_2$  are distinct from the densities for  $N_1 = N_2$  depicted in Fig. 3. The densities for  $N_1 = N_2$  are short-ranged and limited to a finite region of space, viz. Fig. 3. However, in Fig. 4 the density for the component with the larger number of atoms [the component  $i = 1$  in Figs. 4(a)-(b) and the component  $i = 2$  in Figs. 4(c)-(d)] extends over

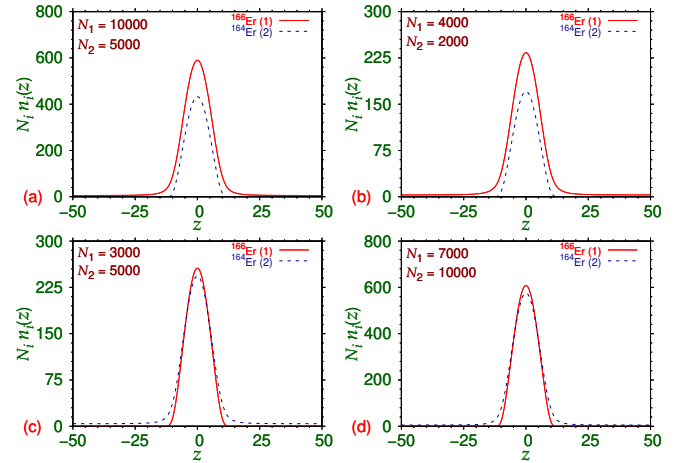


FIG. 4: (Color online) Dimensionless linear density  $N_i n_i(z) \equiv N_i |\psi_{1D}^{(i)}(z)|^2$  of a quasi-1D symbiotic soliton in a binary dipolar BEC of the  $^{166}\text{Er}$ - $^{164}\text{Er}$  mixture for (a)  $N_1 = 10000, N_2 = 5000$ , (b)  $N_1 = 4000, N_2 = 2000$ , (c)  $N_1 = 3000, N_2 = 5000$ , and (d)  $N_1 = 7000, N_2 = 10000$ .

a very large region of space. In Fig. 4, these densities have a small nonzero value up to a very large  $|z|$ . The normalized densities  $n_i(z)$  of the two components in Figs. 4(a)-(b) for  $N_1 > N_2$  are similar, and the same is true for the two components in Figs. 4(c)-(d) for  $N_2 > N_1$  [although the real densities  $N_i n_i(z)$  are proportional to the number of atoms and are different]. In Figs. 4(a)-(b), for  $N_1 > N_2$ , the central density (at  $z = 0$ ) of component 1 is larger than that of component 2 reflecting a larger number of atoms in component 1. In Figs. 4(c)-(d) for  $N_1 < N_2$  the central densities of the two components are practically the same; however, the density of component 2 in these plots has a long “tail” which accounts for a larger number of atoms in this component.

## 2. Quasi-2D symbiotic dipolar soliton

The profile of a quasi-2D dipolar condensate is illustrated in Fig. 1(b). Due to the strong trap in the  $y$  direction the condensate mostly lies in the  $x$ - $z$  plane with a small width in the  $y$  direction. In this quasi-2D model the solitons are two-dimensional and lie strictly in the  $x$ - $z$  plane. The energy versus  $N_1$  phase plot for different  $N_2$  for the formation of a quasi-2D symbiotic dipolar soliton in the  $^{166}\text{Er}$ - $^{164}\text{Er}$  mixture is displayed in Fig. 5. We find that, for  $N_2 = N_1$ , the binding energy of the soliton does not increase linearly with  $N_1$  as in the quasi-1D case depicted in Fig. 2. Although, a quasi-2D symbiotic dipolar soliton can be stabilized for a small  $N_1$ , for large  $N_1 = N_2$  the soliton collapses [16] as indicated by a rapid unbounded increase of the binding energy of the  $N_2 = N_1$  plot for large  $N_1$ . In fact, the numerical routine breaks down for  $N_1 = N_2 > 10000$  signaling a collapse. For a larger  $N_2$  ( $=8000$ ) and a large  $N_1$  ( $N_1 > 10000$ ) the

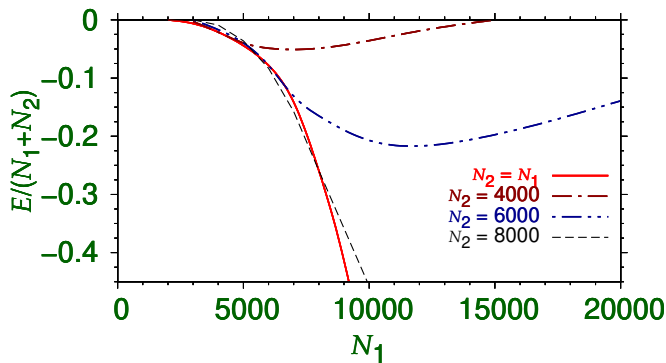


FIG. 5: (Color online) Phase diagram showing the effective energy per atom  $[E/(N_1 + N_2)]$  of a quasi-2D symbiotic dipolar soliton versus the number of atoms  $N_1$  for different  $N_2 - N_2 = N_1, 4000, 6000$  and  $8000$ . The scaling length  $l = 1 \mu\text{m}$  and quasi-2D axial harmonic oscillator length  $d_y = 1/\sqrt{3}$  in dimensionless unit.

system also collapses, due to the large interspecies attraction proportional to  $N_1 N_2$ , as implied by the downward trend of the  $N_2 = 8000$  line in Fig. 5 (not further investigated in this paper). However, when  $N_1$  and  $N_2$  are very different, e.g. for  $N_1 > 8000$  for  $N_2 = 4000$  and for  $N_1 > 10000$  for  $N_2 = 6000$  in Fig. 5, the system is dominated by the repulsive intraspecies interaction of the first component and as  $N_1$  increases the repulsion increases and the energy increases as in Fig. 2 for a quasi-1D symbiotic dipolar soliton. In this self-repulsive system, where each component is dominated by a repulsive intraspecies contact interaction, there is no collapse for large  $N_1$  and for smaller  $N_2$  in Fig. 5 ( $N_2 = 4000$  and  $6000$ ). It is well known that, although there is a collapse in two and three dimensions, there is no collapse in an one-dimensional system [1, 2]. We find that in one dimension the energy decreases linearly with increasing  $N_1$  in Fig. 2, whereas in two dimensions the energy decreases very rapidly to  $-\infty$  for a finite  $N_1$  in Fig. 5 indicating a collapse.

In Figs. 6(a)-(b) we present the contour plot of normalized density  $n_i(x, z) \equiv |\psi_{2D}^{(i)}(x, z)|^2$  of the two components ( $i = 1, 2$ ) of the quasi-2D symbiotic dipolar soliton in the  $^{166}\text{Er}-^{164}\text{Er}$  mixture for  $N_1 = N_2 = 3000$ . The same for  $N_1 = N_2 = 8000$  is displayed in Figs. 6(c)-(d). In contrast to Figs. 4(a)-(b) in the quasi-1D case, where the two densities for  $N_1 = N_2 = 2000$  are quite similar to the two densities for  $N_1 = N_2 = 10000$ , in Figs. 6(a)-(d) the quasi-2D densities of the two components for  $N_1 = N_2 = 3000$  and  $N_1 = N_2 = 8000$  are quite distinct. Because of the collapse instability the densities in Figs. 6(c)-(d) are much larger than those in Figs. 6(a)-(b), as the symbiotic dipolar soliton has contracted significantly for  $N_1 = N_2 = 8000$  indicating a passage to collapse for large  $N_1 = N_2$ . The quasi-2D symbiotic dipolar soliton collapses for  $N_1 = N_2 > 10000$  with divergent quasi-2D densities. From the linear energy dependence in Fig. 2,

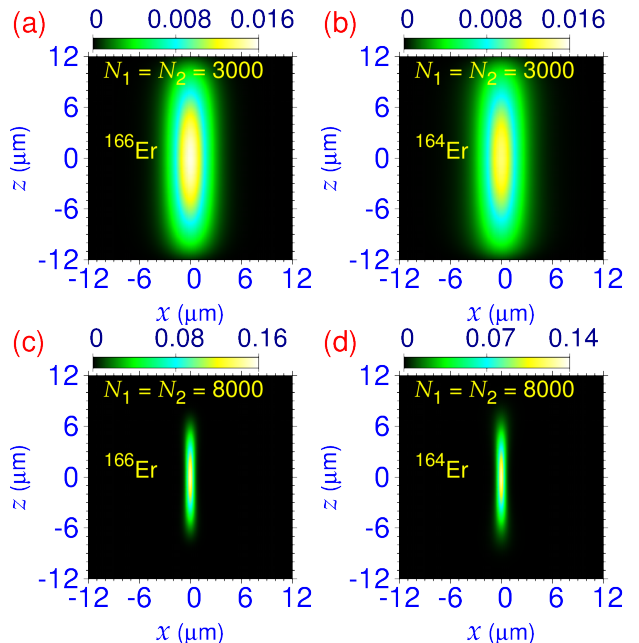


FIG. 6: (Color online) Dimensionless quasi-2D densities  $n_i(x, z) \equiv |\psi_{2D}^{(i)}(x, z)|^2$  of the two components  $i = 1, 2$ , with normalization  $\int d\rho n_i(x, z) = 1$ , of a quasi-2D symbiotic soliton in a binary dipolar  $^{166}\text{Er}-^{164}\text{Er}$  BEC for (a)-(b)  $N_1 = N_2 = 3000$  and (c)-(d)  $N_1 = N_2 = 8000$ .

it was conjectured that the normalized quasi-1D densities of the two components for  $N_1 = N_2$  should be quite similar for different  $N_1$ . Both the nonlinear downward trend of energy in Fig. 5 for  $N_1 = N_2$  as well as the shrinking density pattern in Figs. 6(a)-(d) with increasing  $N_1$  imply the collapse of a quasi-2D symbiotic dipolar soliton for large  $N_1 = N_2$ .

In Figs. 7 we present the contour plot of normalized density  $n_i(x, z)$  for the two components of the quasi-2D symbiotic  $^{166}\text{Er}-^{164}\text{Er}$  soliton in the asymmetric case ( $N_1 \neq N_2$ ) for (a)-(b)  $N_1 = 10000, N_2 = 4000$ , (c)-(d)  $N_1 = 5000, N_2 = 8000$ , and (e)-(f)  $N_1 = 7000, N_2 = 3000$ . In all cases the densities are larger with a smaller spatial extension for the component with smaller number of atoms, e.g., for (b)  $N_2 = 4000$ , (c)  $N_1 = 5000$ , and (f)  $N_2 = 3000$ . In all cases the soliton component with the smaller number of atoms lies in the center of the soliton component with the larger number of atoms. For example, in Figs. 7(c)-(d), the density of the first component in Fig. 7(c) with smaller number of atoms ( $N_1 = 5000$ ) has a smaller spatial extension than that of the second component in Fig. 7(d) with larger number of atoms ( $N_1 = 8000$ ) and the atoms of the first component are surrounded by the atoms of the second component.

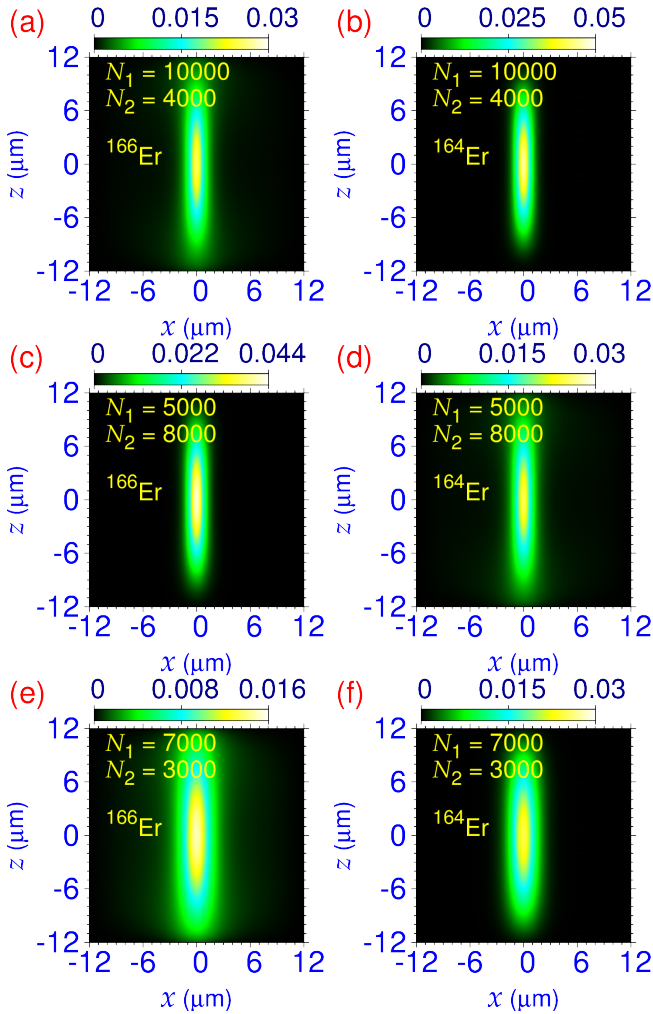


FIG. 7: (Color online) Dimensionless quasi-2D densities  $n_i(x, z) \equiv |\psi_{2D}^{(i)}(x, z)|^2$  of the two components  $i = 1, 2$ , with normalization  $\int d\rho n_i(x, z) = 1$ , of a quasi-2D symbiotic dipolar soliton in a binary dipolar  $^{166}\text{Er}$ - $^{164}\text{Er}$  BEC for (a)-(b)  $N_1 = 10000, N_2 = 4000$ , (c)-(d)  $N_1 = 5000, N_2 = 8000$ , (e)-(f)  $N_1 = 7000, N_2 = 3000$ .

### B. Dynamical stability

Dynamical stability of the quasi-1D and quasi-2D symbiotic dipolar solitons is established by real-time propagation, employing the corresponding converged wave function obtained by imaginary-time propagation as the initial state, after giving a small perturbation to the mean-field model, by changing the interspecies scattering length  $a_{12}$  from 0 to a small negative value. Due to this perturbation, the system becomes more attractive, consequently, the solitons contract and the root-mean-square (rms) sizes reduce. We find that this transition from the initial to the final contracted state is very smooth in nature.

First, we illustrate this transition for the quasi-1D sym-

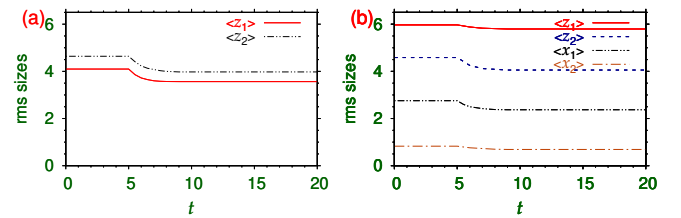


FIG. 8: (Color online) (a) The evolution of rms sizes of the two components  $\langle z_1 \rangle, \langle z_2 \rangle$  of the quasi-1D symbiotic dipolar soliton displayed in Figs. 3(b) for  $N_1 = N_2 = 10000$  as the interspecies scattering length  $a_{12}$  is changed from 0 to  $-2a_0$  at time  $t = 5$ . (b) The evolution of rms sizes of the two components  $\langle x_1 \rangle, \langle x_2 \rangle, \langle z_1 \rangle, \langle z_2 \rangle$  of the quasi-2D symbiotic dipolar soliton displayed in Figs. 7(a)-(b) for  $N_1 = 10000, N_2 = 4000$  as the interspecies scattering length  $a_{12}$  is changed from 0 to  $-a_0$  at time  $t = 5$ .

biotic dipolar soliton, in the  $^{166}\text{Er}$ - $^{164}\text{Er}$  mixture, of Fig. 3(b) for  $N_1 = N_2 = 10000$ , while we introduce a perturbation at  $t = 5$  by changing the interspecies scattering length  $a_{12}$  from 0 to  $-2a_0$ . In Fig. 8(a) we illustrate the evolution of rms sizes  $\langle z_1 \rangle, \langle z_2 \rangle$  of  $^{166}\text{Er}$  and  $^{164}\text{Er}$ , respectively, as obtained by real-time propagation. The rms sizes smoothly evolve from the initial values, at small times ( $t < 5$ ),  $\langle z_1 \rangle = 4.10$  and  $\langle z_2 \rangle = 4.64$  for  $^{166}\text{Er}$  and  $^{164}\text{Er}$ , respectively, to the respective final values  $\langle z_1 \rangle = 3.57$  and  $\langle z_2 \rangle = 3.98$  at large times ( $t > 10$ ). Due to the perturbation at  $t = 5$  the system becomes more attractive and the soliton shrinks resulting in a reduction of the rms sizes.

The same transition for the quasi-2D symbiotic dipolar soliton, in the  $^{166}\text{Er}$ - $^{164}\text{Er}$  mixture, of Fig. 7(a)-(b) for  $N_1 = 10000, N_2 = 4000$  is considered next, while we introduce a perturbation at  $t = 5$  by changing the interspecies scattering length  $a_{12}$  from 0 to  $-a_0$ . In Fig. 8(b) we display the evolution of rms sizes  $\langle z_1 \rangle, \langle x_1 \rangle, \langle z_2 \rangle, \langle x_2 \rangle$ , of  $^{166}\text{Er}$  and  $^{164}\text{Er}$ , respectively, as obtained by real-time propagation. The rms sizes smoothly evolve from the initial values, at small times ( $t < 5$ ),  $\langle z_1 \rangle = 5.97$ ,  $\langle x_1 \rangle = 2.75$  and  $\langle z_2 \rangle = 4.59$ ,  $\langle x_2 \rangle = 0.83$  for  $^{166}\text{Er}$  and  $^{164}\text{Er}$ , respectively, to the respective final values  $\langle z_1 \rangle = 5.80$ ,  $\langle x_1 \rangle = 2.37$  and  $\langle z_2 \rangle = 4.06$ ,  $\langle x_2 \rangle = 0.69$  at large times ( $t > 10$ ). Again due to the perturbation at  $t = 5$ , the symbiotic soliton shrinks leading to a smooth reduction in rms sizes in both  $x$  and  $z$  directions. For both quasi-1D and quasi-2D solitons, the smooth transition of the rms sizes from initial to final values ensures their dynamical stability.

## IV. SUMMARY

We studied the formation of quasi-1D and quasi-2D symbiotic dipolar solitons, in the binary  $^{166}\text{Er}$ - $^{164}\text{Er}$  mixture, bound by an interspecies dipolar interaction, in a self-repulsive binary dipolar BEC, using a numerical so-

lution of the respective reduced mean-field GP equations. To study the effect of the interspecies dipolar interaction on the formation of symbiotic solitons, the interspecies scattering length was kept equal to zero. The experimental scattering lengths in  $^{166}\text{Er}$  and  $^{164}\text{Er}$  are such that each component is dominated by a repulsive contact interaction ( $a > a_{\text{dd}}$ ) [35], and no soliton can be formed in each component in isolation. Only in the presence of the interspecies nonlocal long-range dipolar interaction a symbiotic dipolar soliton in the  $^{166}\text{Er}$ - $^{164}\text{Er}$  mixture is formed. The quasi-1D symbiotic dipolar solitons are mobile along the polarization  $z$  direction of the dipolar atoms and the governing reduced quasi-1D GP equation is obtained by integrating out the  $x$  and  $y$  dependence from the 3D GP equation [41]. The quasi-2D symbiotic dipolar solitons are mobile in the  $x$ - $z$  plane and the governing quasi-2D reduced GP equation is obtained by integrating out the  $y$  dependence from the 3D GP equation [39, 40]. The stationary solitons are obtained by a

numerical solution of the respective model by imaginary-time propagation. The dynamical stability of the solitons is established by a numerical solution of the relevant GP equations by real-time propagation, using the converged solution obtained by imaginary-time propagation as the initial state, after introducing a small perturbation by changing the interspecies scattering length from 0 to a small negative value. Consequently, the binary soliton becomes more attractive and hence contract in size. The transition from the initial soliton state to the final state is found to be smooth, which ensures the dynamical stability of the symbiotic dipolar soliton.

### Acknowledgments

This work is funded partly by the CNPq (Brazil) grant 301324/2019-0.

- 
- [1] Y. S. Kivshar and B. A. Malomed, *Rev. Mod. Phys.* **61**, 763 (1989).
- [2] F. K. Abdullaev, A. Gammal, A. M. Kamchatnov, and L. Tomio, *Int. J. Mod. Phys. B* **19**, 3415 (2005).
- [3] K. E. Strecker, G. B. Partridge, A. G. Truscott, and R. G. Hulet, *Nature (London)* **417**, 150 (2002).
- [4] L. Khaykovich, F. Schreck, G. Ferrari, T. Bourdel, J. Cubizolles, L. D. Carr, Y. Castin, and C. Salomon, *Science* **256**, 1290 (2002).
- [5] S. L. Cornish, S. T. Thompson, and C. E. Wieman, *Phys. Rev. Lett.* **96**, 170401 (2006).
- [6] S. Inouye, M. R. Andrews, J. Stenger, H.-J. Miesner, D. M. Stamper-Kurn, and W. Ketterle, *Nature (London)* **392**, 151 (1998).
- [7] V. M. Pérez-García and J. B. Beitia, *Phys. Rev. A* **72**, 033620 (2005).
- [8] S. K. Adhikari, *Phys. Lett. A* **346**, 179 (2005).
- [9] A. Roeksabutr, T. Mayteevarunyoo, and B. A. Malomed, *Opt. Express* **20**, 24559 (2012).
- [10] S. K. Adhikari and B. A. Malomed, *Phys. Rev. A* **77**, 023607 (2008).
- [11] A. Javed, H. Susanto, R. Kusdiantara, and I. Kourakis, *Eur. Phys. J. Plus* **137**, 1146 (2022).
- [12] S.M. Al-Marzoug, B.B. Baizakov, and H. Bahlouli, *Chaos, Solitons and Fractals* **175**, 114072 (2023).
- [13] X. Ma, R. Driben, B. A. Malomed, T. Meier, and S. Schumacher, *Sci. Rep.* **6**, 34847 (2016).
- [14] S. K. Adhikari, *Phys. Rev. E* **104**, 024207 (2021).
- [15] V. M. Perez-Garcia, H. Michinel, H. Herrero, *Phys. Rev. A* **57**, 3837 (1998).
- [16] L. Bergé, *Phys. Rep.* **303**, 259 (1998).
- [17] R. Y. Chiao, E. Garmire, and C. H. Townes, *Phys. Rev. Lett.* **13**, 479 (1964).
- [18] T. Lahaye, C. Menotti, L. Santos, M. Lewenstein, and T. Pfau, *Rep. Prog. Phys.* **72**, 126401 (2009).
- [19] D. Vudragović, I. Vidanović, A. Balaz, P. Muruganandam, and S. K. Adhikari, *Comput. Phys. Commun.* **183**, 2021 (2012).
- [20] I. Tikhonenkov, B. A. Malomed, and A. Vardi, *Phys. Rev. Lett.* **100**, 090406 (2008).
- [21] V. Galitski and I. B. Spielman, *Nature (London)* **494**, 49 (2013).
- [22] S. Gautam and S. K. Adhikari, *Phys. Rev. A* **91**, 063617 (2015).
- [23] H. Sakaguchi, B. Li, and B. A. Malomed, *Phys. Rev. E* **89**, 032920 (2014).
- [24] H. Sakaguchi and B. A. Malomed, *Phys. Rev. E* **90**, 062922 (2014).
- [25] S. K. Adhikari, *Phys. Rev. A* **103**, L011301 (2021).
- [26] Y.-C. Zhang, Z.-W. Zhou, B. A. Malomed, and H. Pu, *Phys. Rev. Lett.* **115**, 253902 (2015).
- [27] S. Skupin, O. Bang, D. Edmundson, and W. Krolikowski, *Phys. Rev. E* **73**, 066603 (2006).
- [28] A. I. Yakimenko, V. M. Lashkin, and O. O. Prikhodko, *Phys. Rev. E* **73**, 066605 (2006).
- [29] Z. Fan, Y. Shi, Y. Liu, W. Pang, Y. Li, and B. A. Malomed, *Phys. Rev. E* **95**, 032226 (2017).
- [30] M. B. Pandey, P. J. Ackerman, A. Burkart, T. Porenta, S. Žumer, and I. I. Smalyukh, *Phys. Rev. E* **91**, 012501 (2015).
- [31] M. Johansson, A. A. Sukhorukov, and Y. S. Kivshar, *Phys. Rev. E* **80**, 046604 (2009).
- [32] J. Gómez-Gardeñes, B. A. Malomed, L. M. Floría, and A. R. Bishop, *Phys. Rev. E* **74**, 036607 (2006).
- [33] L. E. Young-S., P. Muruganandam, and S. K. Adhikari, *J. Phys. B* **44**, 101001 (2011).
- [34] S. K. Adhikari, *Phys. Rev. A* **90**, 055601 (2014).
- [35] L. Chomaz, I. Ferrier-Barbut, F. Ferlaino, B. Laburthe-Tolra, B. L. Lev, and T. Pfau, *Rep. Prog. Phys.* **86**, 026401 (2023), Table 1.
- [36] E. P. Gross, *Nuovo Cimento* **20**, 454 (1961).
- [37] L. P. Pitaevskii, *Zurn. Eksp. Teor. Fiz.* **40**, 646 (1961) [English Transla.: *Sov. Phys. JETP* **13**, 451 (1961).]
- [38] L. Salasnich, A. Parola, and L. Reatto, *Phys. Rev. A* **65**, 043614 (2002).
- [39] U. R. Fischer, *Phys. Rev. A* **73**, 031602(R) (2006).
- [40] P. Pedri and L. Santos, *Phys. Rev. Lett.* **95**, 200404 (2005).

- [41] S. Sinha and L. Santos, *Phys. Rev. Lett.* **99**, 140406 (2007).
- [42] V. I. Yukalov, *Laser Phys.* **28**, 053001 (2018).
- [43] F. Dalfovo, S. Giorgini, L. P. Pitaevskii, and S. Stringari, *Rev. Mod. Phys.* **71**, 463 (1999).
- [44] P. Muruganandam and S. K. Adhikari, *Comput. Phys. Commun.* **180**, 1888 (2009).
- [45] L. E. Young-S., P. Muruganandam, A. Baláž, S. K. Adhikari, *Comput. Phys. Commun.* **286**, 108669 (2023).
- [46] V. Lončar, L. E. Young-S., S. Škrbič, P. Muruganandam, S. K. Adhikari, A. Baláž, *Comput. Phys. Commun.* **209**, 190 (2016).